Environmental effects in the quantum-classical transition for the delta-kicked harmonic oscillator

A. R. R. Carvalho
Max-Planck-Institut für Physik komplexer Systeme, Nöthnitzer Strasse 38, D-01187 Dresden, Germany

R. L. de Matos Filho and L. Davidovich
Instituto de Física, Universidade Federal do Rio de Janeiro, Caixa Postal 68528, 21941-972 Rio de Janeiro, RJ, Brazil
(Received 24 December 2003; published 24 August 2004)

We discuss the roles of the macroscopic limit and different system-environment interactions in a quantum-classical transition for a chaotic system. We consider the kicked harmonic oscillator subject to reservoirs that correspond in the classical case to purely dissipative or purely diffusive behavior, a situation that can be implemented in ion trap experiments. In the dissipative case, we derive an expression for the time at which quantum and classical predictions become different (breaking time) and show that complete quantum-classical correspondence is not possible in the chaotic regime. For the diffusive environment we estimate the minimum value of the diffusion coefficient necessary to retrieve the classical limit and also show numerical evidence that, for diffusion below this threshold, the breaking time behaves, essentially, like that in the case of a system without a reservoir.

DOI: 10.1103/PhysRevE.70.026211 PACS number(s): 05.45.Mt, 03.65.Yz, 05.45.−a

I. INTRODUCTION

The problem of understanding the classical world from quantum theory is subtle and especially challenging when dealing with classically chaotic systems.

Even the definition of classical chaos cannot be directly translated into quantum mechanics. Exponential sensitivity to initial conditions, used to define classical chaos, relies on the concept of individual trajectories in phase space, which is absent in quantum formalism. The use of classical phase space distributions, instead of trajectories, seems to be the way in which to circumvent this problem, since they can be readily compared with quasiprobability distributions defined for the corresponding quantum system.

One expects, however, that the dynamics of the quantum and the corresponding classical system should differ after some time, even if the initial distributions coincide. This time, often called Ehrenfest time or breaking time, while large for integrable systems, can be very short for chaotic systems. In that case it has been shown [1] to be proportional to the logarithm of the inverse of an effective Planck constant, $\hbar_{\mathrm{eff}}$, which is the ratio between the Planck constant and a typical action of the system. For integrable systems, on the other hand, it scales as an inverse power of $\hbar_{\mathrm{eff}}$. In fact, quantum corrections become important when the distribution is able to explore the nonlinearities of the potential, which can occur on a logarithmic time scale due to the exponentially fast stretching of the distribution imposed by chaotic dynamics.

One way to face this problem is to go to the macroscopic limit, namely, $\hbar_{\mathrm{eff}} \to 0$, which results in an infinite breaking time $\tau_{\hbar}$. Nevertheless, for any physical system, $\hbar_{\mathrm{eff}}$ is not zero and therefore $\tau_{\hbar}$ has a finite value which can be short, even for macroscopic systems. It has been argued that, due to the shortness of the separation time, even components of the solar system would exhibit quantum features, which is in contradiction with observation [2,3].

Reconciliation of quantum and classical predictions in this case is provided by irreversible coupling of the system with an environment [4–6], which leads to elimination of the quantum signatures, so that quantum and classical evolutions remain alike. In systems that, when isolated, exhibit dynamical localization, it was shown [7–10] that noise and dissipation can strongly alter the situation and under certain conditions restore classical-like momentum diffusion. For particular choices of environment, it has also been shown that this reconciliation is possible under some conditions that involve a scaling relation for the effective Planck constant, the nonlinearity parameter and the strength of the system–reservoir interaction [7,10–15].

One of the aims of this paper is to further explore the joint role of the macroscopic limit ($\hbar_{\mathrm{eff}} \ll 1$) and interaction with the environment in the quantum-classical correspondence. In particular, we are also interested in regions where the conditions for classicality do not hold and examine the time scales at which the quantum-classical correspondence breaks down. We should emphasize that this time scale is different from the one in the localization problem studied in Refs. [7–10] since this phenomenom can be absent in the model we consider [16]. Another goal of this paper is to analyze in detail the impact of different forms of the system-environment coupling within the framework of a model that can be implemented experimentally.

To do this, we revisit the kicked harmonic oscillator (KHO), which has been the subject of studies both in classical [17] and quantum descriptions [16,18,19]. Despite some peculiarities and numerical difficulties presented by the KHO, the possibilities for implementation with current available technology for ion traps [20] turn this model into a very attractive one. Moreover, in ion traps, one is able to create artificial reservoirs [21] and different kinds of system–environment interactions have already been produced experimentally [22]. This favorable scenario becomes complete with the possibility of tuning the effective Planck constant by changing experimentally accessible parameters. $\hbar_{\mathrm{eff}}$ and its scaling properties are related to the so-called Lamb–Dicke

parameter (defined later in this paper), which can be modified either by changing the trap frequency or the directions of the laser beams that interact with the ion.

We analyze two limiting cases of environment coupling: zero temperature, which leads in the classical limit to dissipation without diffusion, and a reservoir that leads to diffusion without dissipation. This is not an unrealistic situation: the first may be mimicked by the sideband cooling mechanism in ion traps, under proper conditions, while the second corresponds to white-noise position-independent random force, coupled to the oscillator. The latter of the two is known to be the most important source of decoherence in actual experiments [22]. We present analytical and numerical results concerning the "distance" between quantum and classical predictions and the breaking time. More specifically, in the dissipative case, expressions for the breaking time in three different parameter regions are derived and their physical consequences are discussed. In the most interesting region, we have a result similar to the one obtained recently by Iomin and Zaslavsky [23] using another method. For the diffusive environment we establish the minimum value of the diffusive constant in order to restore classical predictions, and we provide numerical evidence that the breaking time behaves like the one for the system without a reservoir if the diffusion constant is kept below this threshold. We also show that the purely diffusive reservoir has a much stronger impact on the quantum-classical correspondence than the dissipative one.

In Sec. II we present the main features of the classical model, both in the absence and the presence of coupling with the environment. In Sec. III, we introduce the quantum model, and discuss its connection with experimental realization in ion traps and with the corresponding classical model. Section IV is divided into three parts that show the results for the system without a reservoir or one that interacts with dissipative or diffusive reservoirs. Appendices A and B contain detailed derivations of some of the results presented in the body of the text.

II. CLASSICAL DYNAMICS: THE δ-KICKED HARMONIC OSCILLATOR

The classical δ-kicked harmonic oscillator has been studied for both isolated [24] (without a reservoir) and dissipative [25] cases. Here we review the basics features of these models and present also the effects of interaction with a diffusive environment.

A. System without a reservoir

We consider a particle of mass m in a harmonic potential subjected to a sequence of periodically applied δ-like pulses. The Hamiltonian that describes this situation is

$$H = \frac{p^2}{2m} + \frac{m\nu^2 x^2}{2} + A\cos(kx)\sum_n^{\infty}\delta(t - n\tau), \tag{1}$$

where ν is the oscillator frequency, τ the interval between two consecutive kicks and A their amplitude. The kicking potential is position dependent, with periodicity given by the wave vector k.

The differential equations of motion due to this Hamiltonian can be replaced by a discrete map. Between two kicks the system evolves according to

$$\ddot{x} + \nu^2 x = 0, \tag{2}$$

while at kicking times $n\tau$ there is just a shift in momentum, so that

$$x_n^+ = x_n, \quad p_n^+ = p_n + Ak\,\sin(kx), \tag{3}$$

where the variables immediately after and before a kick are indicated, respectively, by the presence or absence of the "+" superscript. After this integration we can connect the solutions before each kick using the following map:

$$x_{n+1} = \cos(\nu\tau)x_n + \sin(\nu\tau)/m\nu[p_n + Ak\,\sin(kx_n)], \tag{4a}$$

$$p_{n+1} = -m\nu\,\sin(\nu\tau)x_n + \cos(\nu\tau)[p_n + Ak\,\sin(kx_n)]. \tag{4b}$$

Using dimensionless variables v and u defined by

$$v = kx,$$

$$u = kp/m\nu, \tag{5}$$

the map becomes

$$v_{n+1} = \cos(\alpha)v_n + \sin(\alpha)[u_n + K\,\sin(v_n)], \tag{6a}$$

$$u_{n+1} = -\sin(\alpha)v_n + \cos(\alpha)[u_n + K\,\sin(v_n)], \tag{6b}$$

where $K = Ak^2/m\nu$ and $\alpha = \nu\tau$ are, respectively, the renormalized kicking strength and the ratio between the period of the kicks and the period of the oscillator. The system's phase space is unbounded and mixed, and exhibits stable islands surrounded by a stochastic web along which the system diffuses. The web is characterized by its thickness that broadens (shrinks) as the value of the chaoticity parameter K increases (decreases). For $\alpha = 2\pi/q$ (q is an integer), the stochastic web displays crystal ($q \in q_c \equiv \{3,4,6\}$), or quasicrystal symmetry ($q \neq q_c$). These basic features can be seen in Fig. 1, where a stroboscopic plot for the map Eqs. (6), is shown for $q=6$ and $K=2.0$ for different initial conditions.

Another useful way in which to study the dynamics is to follow the time evolution of the phase-space probability distribution. This method is especially suitable for problems where the notion of a single deterministic trajectory is absent as in the case of noisy and quantum dynamics. For numerical evaluation of the density dynamics, one usually evolves an ensemble of trajectories generated according to the initial distribution and then, by counting the fraction of trajectories that lies in each cell of phase space, one recovers the density at a given time. However, this method presents some drawbacks in our case, due to the unboundedness of the phase space and the consequent escape of trajectories. One way to get rid of this problem is to extend the phase space boundaries to be sure that, for the time scale one wants to simulate, no trajectories are lost. Nevertheless, increase of the phase space area, keeping the size of the cells constant, requires a larger number of trajectories in order to get good statistics.

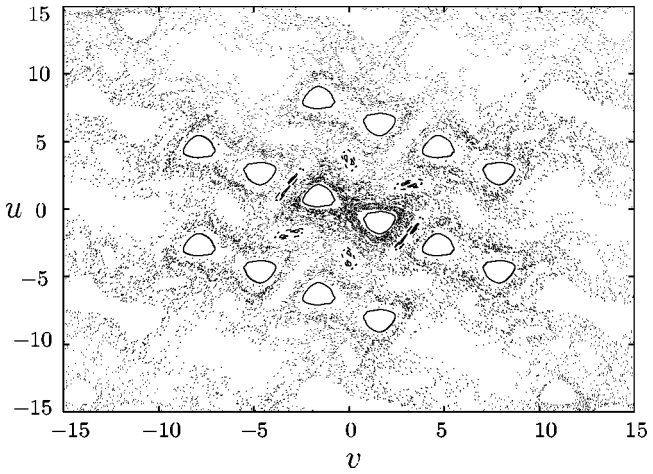

FIG. 1. Stroboscopic plot for $q=6$ and $K=2.0$, showing some stable islands as well as the stochastic web that forms hexagonal symmetry in the unbounded phase space.

This imposes severe constraints on efficient numerical implementation.

Alternatively, we start with a uniformly distributed ensemble of trajectories, each carrying its own weight relative to the initial distribution. According to this, the probability at each point is obtained by requiring that

$$P_n(v_n,u_n) = P_0(v_0,u_0), \tag{7}$$

which means that the value of the initial probability, P_0 at every point (v_0, u_0) in phase space is transported to the image (v_n, u_n) of this point under action of the map Eqs. (6), after n iterations. All the classical quantities calculated throughout the paper are obtained by evaluating each individual trajectory and then averaging them, taking into account their respective probabilities. It is important to mention that, although differences between trajectory-based and true density evolutions are expected [26,27], our simulations show no difference between the two methods for sufficiently small phase-space partitions.

Figure 2 displays the evolution of an initial Gaussian probability distribution centered at the origin for the same parameters of Fig. 1. The numerical procedure used to plot the distributions is similar to the one described to calculate the averages but, in order not to have problems with dispersion of the trajectories from neighboring regions in phase space at $t=0$, we do the calculation backwards in time, choosing the grid at any instant of time t and evolving the points using the inverse map to find the probability of the inverse image of this point at $t=0$.

From Fig. 2 one can identify the inner structure present in Fig. 1. The whole web structure would be visible if there were a larger number of kicks.

B. Dissipative case

The dynamics of the kicked oscillator change if a dissipation mechanism is introduced. In our model this can be achieved by modifying the equation of motion between the kicks, Eq. (2), with the addition of a friction term proportional to the velocity,

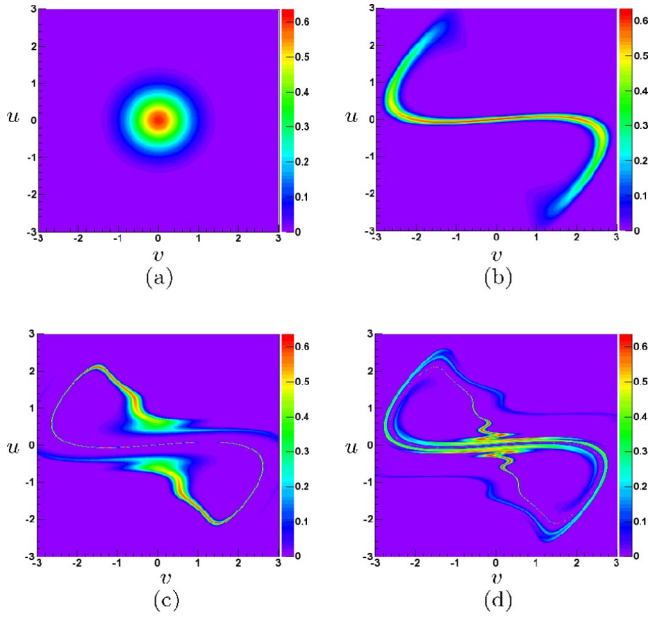

FIG. 2. (Color online) Classical probability distribution for $q=6$ and $K=2.0$ after zero (a), three (b), six (c) and nine (d) kicks. The same structure of the trajectory-based stroboscopic map as that in (Fig. 1) is shown. After nine kicks only the central structure is visible. The whole web structure would be seen if there were a larger number of kicks.

$$\ddot{x} + \nu^2 x + \Gamma\dot{x} = 0, \tag{8}$$

where Γ is the dissipation rate. The discrete map obtained by integration of Eq. (8) and use of the shift in momentum, Eq. (3), is

$$x_{n+1} = e^{-\Gamma\pi/2}\left\{\cos(\overline{\alpha})x_n + \frac{\sin(\overline{\alpha})}{m\ \Omega}[p_n + Ak\ \sin(kx_n)]\right\}, \tag{9a}$$

$$p_{n+1} = e^{-\Gamma\pi/2}\{-m\Omega\ \sin(\overline{\alpha})x_n + \cos(\overline{\alpha})[p_n + Ak\ \sin(kx_n)]\}, \tag{9b}$$

where

$$\Omega = \sqrt{\nu^2 - \Gamma^2/4},$$

$$p_n/m = \dot{x} + \Gamma x/2, \tag{10}$$

$$\overline{\alpha} = \Omega\tau.$$

We again perform a change to dimensionless variables v' and u', so that now

$$v' = kx,$$

$$u' = kp/m\Omega, \tag{11}$$

and

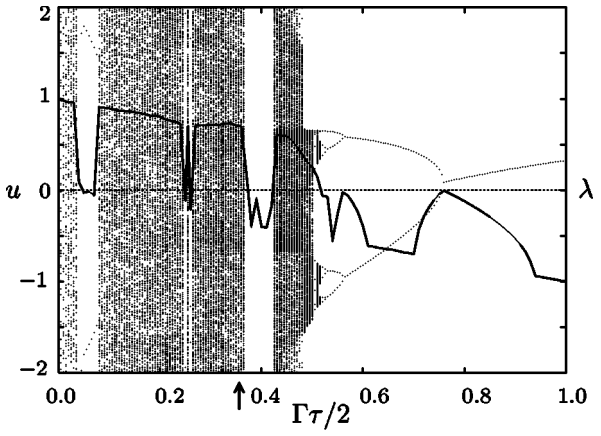

FIG. 3. Average Lyapunov exponent λ (solid line) and bifurcation diagram (dots) as a function of the dissipation parameter $\Gamma\tau/2$ for $K'=6.0$ and $q=6$. The horizontal line at $u=0$ was plotted as a reference for the Lyapunov exponent. For the bifurcation diagram, the vertical axis corresponds to the last 10^3 points of u after 10^6 iterations of the map, Eqs. (12). We only show the region from −2 to 2 for clarity. The arrow refers to the case plotted in Fig. 4.

$$v'_{n+1} = e^{-\Gamma\tau/2}\{\cos(\overline{\alpha})v'_n + \sin(\overline{\alpha})[u'_n + K' \sin(v'_n)]\}, \tag{12a}$$

$$u'_{n+1} = e^{-\Gamma\tau/2}\{-\sin(\overline{\alpha})v'_n + \cos(\overline{\alpha})[u'_n + K' \sin(v'_n)]\}, \tag{12b}$$

where $K'=Ak^2/m\Omega$.

There are new scenarios that arise from the addition of dissipation depending on the values of K' and $\Gamma\tau$. When one of these parameters is changed, the system may change from periodic to chaotic motion in a sequence of period-doubling bifurcations [28]. In Fig. 3 we show this sequence and also the average Lyapunov exponent for $K'=6.0$ and $\Gamma\tau/2$ varying from 0 to 1. For the bifurcation diagram we iterated the map, Eqs. (12), for 10^6 steps and plotted the last 10^3 points that correspond to the u variable on the vertical axis. The Lyapunov exponent is averaged over 10^4 different initial conditions equally distributed around the origin, taking into account the same initial probability distribution as in Fig. 2. For each trajectory the exponent is calculated using the procedure described in Ref. [29] for 10^6 iterations. One can clearly identify the periodic regions corresponding to non-positive Lyapunov exponents and the chaotic ones where the system goes to strange attractors like the one shown in Fig. 4.

C. Diffusive case

Another kind of external disturbance that can affect the oscillator dynamics is diffusion generated by noise due, for example, to fluctuating forces that act on the system. One possible mathematical description for the evolution of the probability distribution between two consecutive kicks is the Fokker–Planck equation,

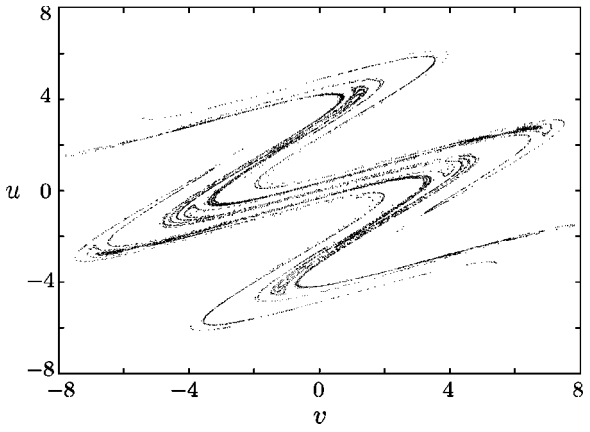

FIG. 4. Strange attractor obtained from the map, Eqs. (12), for $q=6$, $K'=6.0$ and $\Gamma\tau/2=0.36$ corresponding to a Lyapunov exponent of 0.697 in Fig. 3 (denoted by an arrow there).

$$\frac{\partial P}{\partial t} = \nu u\frac{\partial P}{\partial v} - \nu v\frac{\partial P}{\partial u} + \mathcal{D}\left(\frac{\partial^2 P}{\partial v^2} + \frac{\partial^2 P}{\partial u^2}\right). \tag{13}$$

The first two terms describe the harmonic evolution while the third accounts for diffusion, in both v and u, with diffusion coefficient $\mathcal{D}$. This diffusive term has two different effects on the system's dynamics. First, noise limits the development of small-scale structures in phase space generated by the nonlinear dynamics, thereby smoothing out the probability distribution. While stretching of the distribution tends to generate thin structures in phase space, noise will tend to counterbalance this effect, leading to a lower limit in the width of such structures which will depend on both the nonlinearity parameter and the strength of the noise [12]. The second effect is a faster spread of the system over phase space. In fact, the diffusion produced by noise adds a new mechanism for connecting different parts of the web, thus enhancing the original chaotic diffusion.

III. QUANTUM DYNAMICS: QUANTUM δ-KICKED HARMONIC OSCILLATOR

A. System without a reservoir

The quantum Hamiltonian for the δ-kicked harmonic oscillator is given by replacing in Eq. (1) the variables x and p by operators,

$$\hat{H} = \frac{\hat{p}^2}{2m} + \frac{m\nu^2\hat{x}^2}{2} + \hbar K_q \cos(k\hat{x})\sum_n^{\infty}\delta(t-n\tau), \tag{14}$$

where we have defined $K_q=A/\hbar$.

It was shown in Ref. [20] that this model describes the center-of-mass motion of an ion in a one-dimensional harmonic trap subjected to a sequence of standing-wave laser pulses, off-resonant with respect to a transition between the ground state and another electronic level. In this off-resonance condition the excited state is negligibly populated and can be eliminated adiabatically. The result of this elimination is an equation that describes just the motional dynamics subject to recoil associated to incoming laser pulses.

In terms of the annihilation and creation operators $\hat{a}$ and $\hat{a}^\dagger$ for the harmonic oscillator,

$$\hat{a} = \sqrt{m\nu/2\hbar}\hat{x} + i\sqrt{1/2\hbar m\nu}\hat{p}, \tag{15}$$

the above Hamiltonian can be written as

$$\hat{H} = \hbar\nu\hat{a}^\dagger\hat{a} + \hbar K_q \cos[\eta(\hat{a}+\hat{a}^\dagger)]\sum_n^\infty \delta(t-n\tau), \tag{16}$$

where

$$\eta = k\sqrt{\hbar/2m\nu} \tag{17}$$

is a scaling parameter related to the macroscopic limit, the so-called Lamb–Dicke parameter [30]. This parameter can be expressed as $\eta = 2\pi\Delta x_0/\lambda$, where Δx_0 is the width of the ground state of the harmonic oscillator,and $\lambda = 2\pi/k$ is the wavelength of the kicking force. This is the classicality parameter for the model under consideration. Its square is seen to be the ratio between $\hbar$ and the action $2m\nu/k^2$, and it plays the role of dimensionless parameter $\hbar_{\text{eff}}$ mentioned in Sec. I. The limit $\eta \to 0$ can be achieved by letting $k \to 0$. This parameter can be easily changed in ion trap experiments by varying the direction of the kicking laser pulses with respect to the trap axis, since k stands, in this case, for the projection of the lasers wave vectors on the trap axis.

In terms of η, we can write

$$\langle\hat{a}\rangle = \frac{1}{2\eta}(v+iu) \equiv (\overline{v}+i\overline{u}), \tag{18}$$

$$K_q = \frac{K}{2\eta^2}, \tag{19}$$

where Eqs. (5), (15), and (17) were used. While the classicality parameter η appears naturally in the quantum model when it is expressed in terms of the annihilation and creation operators, it may also be introduced classically by using the new variables $\overline{v}$ and $\overline{u}$, which yield the following scaled map:

$$\overline{v}_{n+1} = \cos(\alpha)\overline{v}_n + \sin(\alpha)\left[\overline{u}_n + \frac{K}{2\eta}\sin(2\eta\overline{v}_n)\right], \tag{20a}$$

$$\overline{u}_{n+1} = -\sin(\alpha)\overline{v}_n + \cos(\alpha)\left[\overline{u}_n + \frac{K}{2\eta}\sin(2\eta\overline{v}_n)\right]. \tag{20b}$$

On the quantum level, the evolution dictated by Eq. (16) can be written as a map that connects the state of the system before each consecutive kick as

$$|\psi\rangle_{n+1} = \hat{U}_h\hat{U}_k|\psi\rangle_n = e^{-i\nu\pi\hat{a}^\dagger\hat{a}}e^{-iK_q\cos[\eta(\hat{a}+\hat{a}^\dagger)]}|\psi\rangle_n, \tag{21}$$

where $\hat{U}_h$ and $\hat{U}_k$ are, respectively, the evolution operators for the harmonic oscillator and for the kicks.

B. Open system: Influence of environment

The influence of the environment on the system can be described by the master equation,

$$\frac{d\hat{\rho}}{dt} = -\frac{i}{\hbar}[\hat{H},\hat{\rho}] + \mathcal{L}\hat{\rho}, \tag{22}$$

where $\hat{\rho}$ is the reduced density operator of the system in the interaction picture. The first term on the right-hand side of Eq. (22) corresponds to the unitary dynamics while the second term represents the nonunitary effect of the environment in Lindblad form,

$$\mathcal{L}\hat{\rho} \equiv \sum_i (\gamma_i/2)(2\hat{c}_i\hat{\rho}\hat{c}_i^\dagger - \hat{c}_i^\dagger\hat{c}_i\hat{\rho} - \hat{\rho}\hat{c}_i^\dagger\hat{c}_i). \tag{23}$$

Operators $\hat{c}_i$ are related to the form of system-environment coupling and constants γ_i measure the strength of the coupling.

Equation (23) is frequently found in a description of dissipative systems. It can be derived under very general assumptions, namely, "Markovicity" and complete positivity of the time evolution of the reduced density operator of the system [31,32]. This latter condition is defined in the following way. Let A be the system for which the reduced density operator is defined, $\mathcal{H}_A$ the corresponding Hilbert space, and Λ_A the time-evolution map for the reduced density operator ρ. Consider any possible extension of $\mathcal{H}_A$ to the tensor product $\mathcal{H}_A \otimes \mathcal{H}_B$, where $\mathcal{H}_B$ is any arbitrary Hilbert space; then Λ_A is completely positive on $\mathcal{H}_A$ if $\Lambda_A \otimes I_B$ is positive for all such extensions. Complete positivity corresponds to the statement that, if system A evolves and system B does not, any initial density matrix of the combined system evolves into another density matrix.

In trapped ions one can use the technique of "reservoir engineering" [21–23] to build different kinds of $\hat{c}_i$ operators for center-of-mass motion of the ion, and, in particular, the dissipative and diffusive reservoirs discussed previously in the context of classical dynamics.

1. Dissipative case

Dissipation by a zero-temperature reservoir in the weak coupling limit ($\Gamma \ll \nu$) and in the rotating-wave approximation is described by Eq. (22) using just one operator, $\hat{c}_1 \equiv \hat{a}$,

$$\frac{d\hat{\rho}}{dt} = -\frac{i}{\hbar}[\hat{H}',\hat{\rho}] + \frac{\Gamma}{2}(2\hat{a}\hat{\rho}\hat{a}^\dagger - \hat{a}^\dagger\hat{a}\hat{\rho} - \hat{\rho}\hat{a}^\dagger\hat{a}), \tag{24}$$

where $\hat{H}'$ has the same form as $\hat{H}$ given by Eq. (16), with ν replaced by the frequency Ω given by Eq. (10). We will see that, with this choice, the oscillation frequencies of the quantum and classical systems will coincide.

From master equation (24), one gets the equations of motion for the expectation values between kicks:

$$\langle\dot{\hat{a}}\rangle = \mathrm{Tr}(\hat{a}\dot{\hat{\rho}}) = -i\Omega\langle\hat{a}\rangle - \frac{\Gamma}{2}\langle\hat{a}\rangle, \tag{25}$$

which can be written in terms of $\hat{x}$ and $\hat{p}$ as

$$\langle\dot{\hat{x}}\rangle = \frac{\langle\hat{p}\rangle}{m} - \frac{\Gamma}{2}\langle\hat{x}\rangle, \tag{26}$$

$$\langle\dot{\hat{p}}\rangle = -m\Omega^2\langle\hat{x}\rangle - \frac{\Gamma}{2}\langle\hat{p}\rangle. \tag{27}$$

One should note that, different from classical equations of motion, dissipation appears here in a symmetric way with respect to position and momentum. This is related to the rotating-wave approximation, adopted in deriving Eq. (24): this approximation requires that the oscillator undergoes many oscillations within the decay time (that is, one should have $\Gamma \ll \nu$), which implies that effect of dissipation gets distributed between the canonical coordinates.

Taking the derivative of Eq. (26) and using Eq. (27) one gets

$$\langle \ddot{\hat{x}} \rangle + \left(\Omega^2 + \frac{\Gamma^2}{4} \right) \langle \hat{x} \rangle + \Gamma \langle \dot{\hat{x}} \rangle = 0. \tag{28}$$

Using Eq. (10), we can see that this equation that describes the quantum dynamics between kicks is identical to its classical version, Eq. (8), so the quantum and the classical systems oscillate with the same frequency.

2. Diffusive case

The purely diffusive reservoir master equation can be obtained from Eq. (22) by choosing two operators, $\hat{c}_1 = \hat{a}$ and $\hat{c}_2 = \hat{a}^\dagger$, with the same rate, $\gamma_1 = \gamma_2 = \gamma$,

$$\dot{\hat{\rho}} = \frac{\gamma}{2} [(2\hat{a}\hat{\rho}\hat{a}^\dagger - \hat{a}^\dagger \hat{a}\hat{\rho} - \hat{\rho}\hat{a}^\dagger \hat{a}) + (2\hat{a}^\dagger \hat{\rho}\hat{a} - \hat{a}\hat{a}^\dagger \hat{\rho} - \hat{\rho}\hat{a}\hat{a}^\dagger)]. \tag{29}$$

This is a combination of cooling and heating reservoirs and due to the fact that they have the same rates, all terms that lead to drifting are canceled out and only diffusion terms survive. This becomes clear when one explicitly writes the corresponding Fokker–Planck equation for the Wigner function:

$$\frac{\partial W}{\partial t} = \gamma \frac{\partial^2 W}{\partial \alpha \, \partial \alpha^*}, \tag{30}$$

or, in terms of $\overline{v}$ and $\overline{u}$,

$$\frac{\partial W}{\partial t} = \frac{\gamma}{4} \left(\frac{\partial^2}{\partial \overline{v}^2} + \frac{\partial^2}{\partial \overline{u}^2} \right) W. \tag{31}$$

Equation (31) is equivalent to the third term of Eq. (13) rewritten in terms of the rescaled variables if we set $\gamma = \mathcal{D}/\eta^2$.

A purely diffusive reservoir can be produced by random electric fields [33,34] and it is known to model heating of the vibrational energy observed in recent experiments on ion dynamics [22].

IV. RESULTS

The classical description of a chaotic dynamical system, either using single trajectories or a probability distribution, is based on the analysis of phase space and its structures. The definition of a single trajectory in the quantum case is prevented by the uncertainty principle so a suitable description of the system is based on quasiprobability distributions. The Wigner function fulfills almost all the requirements for being a true probability distribution, as it is the only quantum distribution that yields the correct marginal distributions for any direction of integration in phase space, however it can exhibit negative values. For our purposes, this turns out to be an advantage, because it highlights the differences between quantum and classical dynamics. As a matter of fact, it is much easier to detect quantum signatures with the Wigner distribution than with the Husimi or Q functions.

Oscillations between negative and positive values in the Wigner function are a sign of the existence of quantum interference phenomena, which are absent in its classical counterpart. The role played by decoherence in washing out interference patterns is also easily visualized in the Wigner function [15]. More than a visualization tool, the Wigner function can be useful to derive some analytical results concerning the quantum-classical limit.

In what follows we make use of the Wigner function and of its Fourier transform, the characteristic function, to obtain new results concerning time scales for the quantum-classical transition. By combining the interaction with the environment and the possibility of varying the effective Planck constant, we are able to discuss not only the regions of parameters for the classical limit but also the behavior of breaking time in open systems.

A. System without a reservoir

In the absence of interaction with the environment, the classical limit is investigated by changing the scaling parameter η. One should mention that, in terms of the variables $\overline{u}$ and $\overline{v}$, the initial distribution does not depend on η, and is taken to be the same for the classical and quantum systems. Of course, in terms of the original variables u and v, decreasing η leads to shrinkage in the width of the initial distribution in both the classical and the quantum situations. In any case, changing η will affect both the classical and quantum solutions, since the initial states are always taken to coincide, and a broader initial packet will explore, from the beginning, a larger region of phase space.

In Fig. 5 we show the Wigner function for $\eta = 0.5$ (top) and 0.1 (bottom) after nine kicks, corresponding to, respectively, the classical situation depicted in Fig. 2(d) and its scaled version (not shown). By decreasing the value of the effective Planck constant one gets a quantum phase space that resembles more and more the overall classical structure but still with the presence of interference patterns.

After some time these differences between quantum and classical evolutions become important and estimates can be made using the characteristic function $C(\lambda, \lambda^*)$, defined as

$$C(\lambda, \lambda^*) = \mathrm{Tr}[\hat{\rho} e^{\lambda \hat{a}^\dagger - \lambda^* \hat{a}}]. \tag{32}$$

Expanding the exponential of the cosine function in the quantum map, Eq. (21), in terms of Bessel functions, it is possible to explicitly write the characteristic function after the nth kick in terms of its initial value, $C_0(\lambda_n, \lambda_n^*)$, as [18]

$$C_n(\lambda, \lambda^*) = \sum_{m_1, \ldots, m_n = -\infty}^{\infty} J_{m_1}(z_1) J_{m_2}(z_2) \ldots J_{m_n}(z_n) C_0(\lambda_n, \lambda_n^*), \tag{33}$$

where

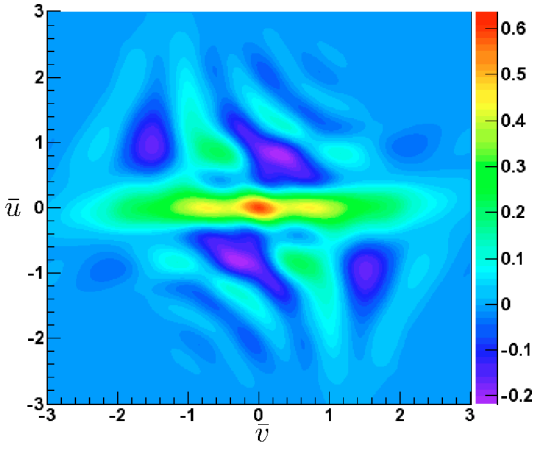

(a)

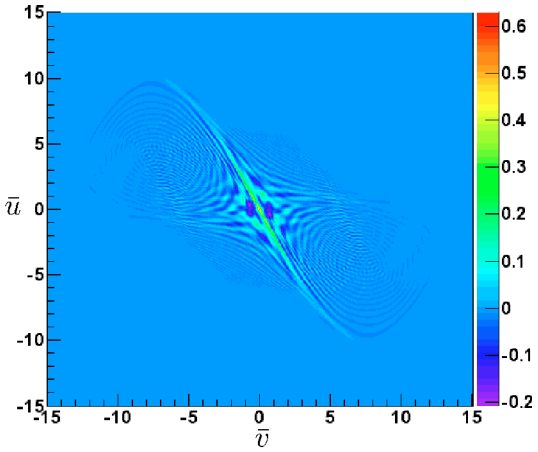

(b)

FIG. 5. (Color online) Wigner distribution after nine kicks for $\eta=0.5$ (a) and 0.1 (b). In both cases the Wigner function presents negative values but as the Lamb–Dicke parameter is decreased (as it gets closer to the classical limit) there is better correspondence with the overall classical structure shown in Fig. 2(d).

$$\lambda_k = \lambda_{k-1} e^{i\alpha} + i m_k \eta, \tag{34a}$$

$$z_k = 2K_q \sin(\xi_k) = \frac{K}{\eta^2}\sin(\xi_k), \tag{34b}$$

$$\xi_k = -\frac{\eta}{2}(\lambda_k + \lambda_k^*), \tag{34c}$$

$$\lambda_0 \equiv \lambda, \tag{34d}$$

J_m are Bessel functions and $\alpha=\nu\tau$, as in the classical case.

It is interesting to compare Eq. (33) with the corresponding one for the classical system, which can be obtained by introducing the classical map Eqs. (20), into the appropriate classical definition of the characteristic function. This definition follows from the quantum expression, Eq. (32), upon replacing the trace by a double integral, the operators by complex numbers and the density matrix by a classical probability density. One gets then

$$C_n^{(\mathrm{cl})}(\lambda,\lambda^*) = \sum_{m_1,\ldots,m_n=-\infty}^{\infty} J_{m_1}\left(\frac{K}{\eta^2}\xi_1\right)\ldots J_{m_n}\left(\frac{K}{\eta^2}\xi_n\right) \times C_0(\lambda_n,\lambda_n^*). \tag{35}$$

It is clear that the classical expression is obtained from the quantum one when $|\xi_k| \ll 1$, in which case

$$\sin(\xi_k) \approx \xi_k. \tag{36}$$

Since, according to Eq. (34a), ξ_k is proportional to η, this approximation should hold for sufficiently small η in the beginning of evolution of the system. However, as time evolves, and $|\lambda_k|$ grows, it eventually ceases to be true. This is precisely where the breakdown between classical and quantum evolution occurs.

An expression for the breaking time can be obtained by comparing the quantum and classical characteristic functions. We define it as the time at which the approximation, Eq. (36), fails, or, in other words, at which $\xi_k \approx 1$. Assuming a strong chaos condition ($K \gg 1$), one is able to derive [18]

$$\tau_\hbar \approx \frac{\ln(2\bar{K}/\eta)}{\ln(\bar{K})}, \tag{37}$$

where $\bar{K}=K\sin(\alpha)$. This result displays scaling of the breaking time with the logarithmic of $1/\eta^2$, which stands for the $\hbar_{\mathrm{eff}}^{-1}$ already mentioned in Sec. I. A numerical check of this expression needs an operational definition for the breaking time, which involves, also, the choice of an appropriate measure of the distance between quantum and classical systems. Information measures that can be used to compare two different distributions are available in the literature [35], and have been applied in the context of quantum-classical transition for chaotic systems [14]. Measures based on a comparison between whole distributions, although more complete, would lead to a large increase in computational time and experimental difficulties. Although the Wigner function has already been measured in experiments with trapped ions [36], it would be challenging to resolve details of the interference fringes seen, for example, in Fig. 5(b). The relative distance between the classical ($\langle\Delta\bar{v}_{cl}^2\rangle$) and quantum ($\langle\Delta\bar{v}_q^2\rangle$) variances of the distributions, defined as

$$d_r = \left|\frac{\langle\Delta\bar{v}_{cl}^2\rangle - \langle\Delta\bar{v}_q^2\rangle}{\langle\Delta\bar{v}_{cl}^2\rangle}\right|, \tag{38}$$

is a much simpler quantity that already shows the scaling properties of Eq. (37). Figure 6 shows the classical and quantum variances (left panels) and the relative distance d_r (right panels) as a function of the number of kicks for two different Lamb–Dicke parameters. The separation time is defined as the time at which the relative distance crosses a given value ϵ ($\epsilon=0.1$ in Fig. 6). In Fig. 7 we plot $\tau_\hbar$ obtained in this way as a function of $\ln(1/\eta)$ and, although the absolute value of the breaking time depends on the choice of ϵ, tests with ϵ ranging from 5% to 30% show only slight modifications in the curves and confirm the scaling behavior, Eq. (37), independent of the particular definition of separation.

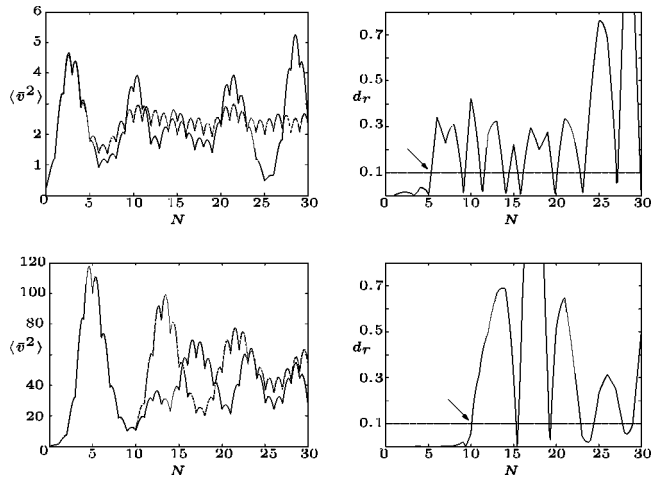

FIG. 6. Classical and quantum variances (left panels) and the relative distance d_r (right panels) as a function of the number of kicks for $\eta=0.5$ (top) and 0.1 (bottom). The quantum variance (solid line) remains close to the classical (dashed line) for a longer time when the Lamb–Dicke parameter is smaller. The breaking time, indicated by arrows, corresponds to the instant at which the relative distance gets larger than a chosen value, $\epsilon=0.1$ (horizontal line in the right panels).

B. Dissipative environment

The analytical solution for the quantum dissipative problem in terms of the characteristic function is also given by Eq. (33) and the only change affects the relation, Eq. (34a), that must be replaced by

$$\lambda_k = \lambda_{k-1} e^{i\bar{\alpha}} e^{-\Gamma\tau/2} + i m_k \eta, \tag{39}$$

where Γ was introduced in the classical case. Besides the usual rotation due to harmonic motion represented by the complex exponential in Eq. (39) there is also exponential decay due to dissipative drift in the characteristic function argument [37].

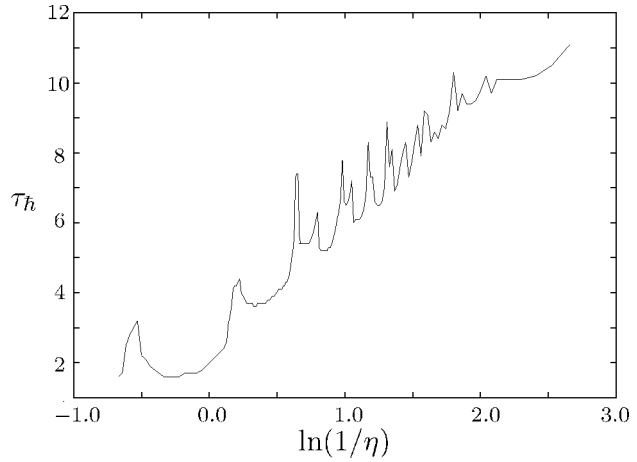

FIG. 7. Breaking time as a function of $\ln(1/\eta)$ for $K=2.0$ and $q=6$. Despite the oscillations there is clear linear behavior, thus confirming the scaling predicted by Eq. (37).

TABLE I. Breaking time for dissipative dynamics in four different regions of parameters $\Gamma\tau/2$, η and $\bar{K}'$.

Nonlinearity strength	Deep quantum regime	Weak quantum regime
	$\Gamma\tau/2 < \ln(\eta/2)$	$\Gamma\tau/2 > \ln(\eta/2)$
$\ln(\bar{K}') > \Gamma\tau/2$	(a) $\tau_\hbar \approx 1$ kick	(c) $\tau_\hbar \approx \dfrac{\ln(2\bar{K}'/\eta)}{\ln(\bar{K}') - \Gamma\tau/2}$
$\ln(\bar{K}') < \Gamma\tau/2$	(b) $\tau_\hbar \approx 1$ kick	(d) $\tau_\hbar \to \infty$

In analogy to what was done for the system without a reservoir, one can obtain the breaking time by examining when the quantum characteristic function can no longer be described by its semiclassical approximation. This procedure is fully described in Appendix A and the results are summarized in Table I. The first column in Table I represents a region characterized by a deep quantum regime where a classical description of the system is already not valid right after the first kick, for all finite values of the dissipation. It is interesting to note that, in this region, quantum-classical correspondence is lost even if dissipation is sufficient to bring the classical system into a periodic regime.

In the second column in Table I we have the most interesting range of parameters for the quantum-classical transition (we call it the "weak quantum regime"), where two different regimes exist: one indicates an increase of the breaking time with dissipation, and the other showing close quantum-classical behavior for all times ($\tau_\hbar \to \infty$). This latter case corresponds to a situation where dissipation is so strong that classical chaos is suppressed and the system goes to a simple attractor. The breaking time for region (c) in Table I,

$$\tau_\hbar^{\mathrm{dis}} \approx \frac{\ln(2\bar{K}'/\eta)}{\ln(\bar{K}') - \Gamma\tau/2}, \tag{40}$$

with $\bar{K}' = K' \sin(\bar{\alpha})$, increases as dissipation coefficient grows, but it keeps the same logarithmic-scale dependence with respect to the effective Planck constant as in the case without a reservoir.

Although $\tau_\hbar^{\mathrm{dis}}$ can be arbitrarily large, as pointed out by Iomin and Zaslavsky [23] in recent derivation of an expression similar to Eq. (40), this is not the case if one wants to preserve a strange attractor. The condition $\Gamma\tau/2 = \ln(\bar{K}')$, which separates regions (c) and (d) in Table I, corresponds to the situation where the origin of phase space changes from an unstable point to a stable fixed point. However, instability of the origin is not sufficient to ensure chaotic dynamics. Indeed, Fig. 3 exhibits a large range of values of $\Gamma\tau/2$ for which the system is attracted to some periodic trajectory, even when $\Gamma\tau/2 < \ln(K)$.

The ratio between the breaking times with and without dissipation is given by

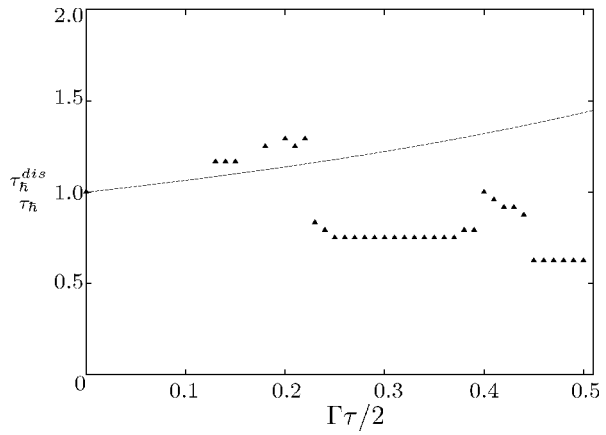

FIG. 8. Ratio between the breaking time with and without dissipation as a function of $\Gamma\tau$ for the same parameters as in Fig. 3 and $\eta=0.5$. The solid line shows the analytical prediction, Eq. (41), while triangles show numerical simulations that compare quantum and classical systems. The differences between quantum and classical environments are responsible for the deviations observed for larger values of $\Gamma\tau$. Smaller values of $\Gamma\tau$ were not considered due to numerical constraints.

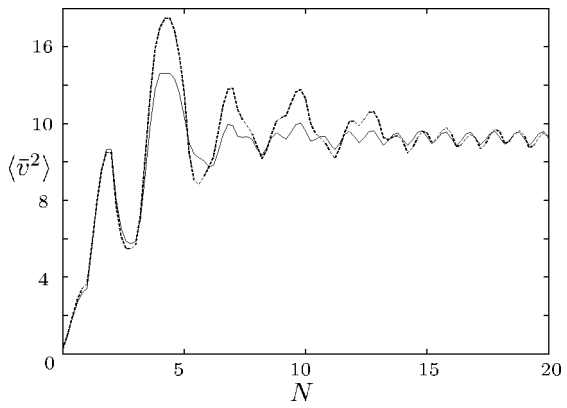

FIG. 9. Classical (dashed line) and quantum (solid line) evolution of $\langle\Delta\bar{v}^2\rangle$ as a function of the number of kicks N for $K'=6.0$ and $\Gamma\tau/2=0.36$. Classical and quantum variances show the same asymptotic behavior despite the fact that they can differ in a transient regime.

$$\frac{\tau_\hbar^{\mathrm{dis}}}{\tau_\hbar} \approx \frac{\ln(\overline{K'})}{\ln(\overline{K'}) - \Gamma\tau/2}. \tag{41}$$

This expression exhibits the increase of breaking time as a function of $\Gamma\tau$. In Fig. 8 this relation is plotted together with numerical simulations for $K'=6.0$ with the horizontal axis ending at the value $(\Gamma\tau/2)_{\max}\approx 0.51$ of the dissipation constant, for which the Lyapunov exponent becomes negative (see Fig. 3). For this value of kicking strength the maximum increase in breaking time is around 1.5 and therefore it does not help considerably in achieving the classical limit. This increase depends on the values of the chaoticity parameter but even for very large values ($K'\approx 500$) it is less than a factor of 4.

Although expression (41) is independent of scaling parameter η, some remarks about the role played by the macroscopic limit in the dissipative case are needed. It should be noted that the quantum description of a zero-temperature reservoir given by Eq. (24) is not completely equivalent to the classical description based on the map, Eqs. (12). In fact, a classical distribution subjected to only dissipative dynamics would shrink to a point located at the origin, while a quantum distribution would end up in the ground state, which has a finite width due to the uncertainty principle. This argument does not invalidate the results presented in Table I, but instead emphasizes that they are valid for the semiclassical approximation that is not equivalent to the fully classical system based on the map, Eqs. (12).

This also provides an explanation for the deviations between numerical and analytical results shown in Fig. 8. Only in a small range of dissipation strength ($0.12\lesssim\Gamma\tau/2\lesssim 0.22$) were we able to see the expected growth in breaking time, while for larger values of $\Gamma\tau/2$, the effects of the difference between classical and quantum systems, discussed above, become dominant.

It is interesting to note the sudden growth in breaking time for the region corresponding to the periodic window around $\Gamma\tau/2=0.4$ shown in Fig. 3. This should be expected, since quantum and classical systems should stay together for a longer time outside the chaotic region. On the other hand, as $\Gamma\tau$ increases, inside the same region, one notices that the breaking time decreases. This is due to the fact that, for larger dissipation, the distribution shrinks at a faster rate, implying that the two distributions approach at an earlier time the region around the origin, where the uncertainty principle plays a dominant role.

For smaller values of dissipation parameter, the system could spread over a large region of phase space and require a huge amount of computational resources. This, together with reliability problems for even smaller values of $\Gamma\tau/2$, imposed the limit $\Gamma\tau/2\gtrsim 0.12$ for the dissipation parameter in our calculations.

It is important to understand the meaning of breaking time and its consequences for dynamics of the system at different times. In particular, the stationary state produced by dissipation is of much interest and this issue of long time behavior has been addressed before in the case of the standard map [8]. The existence of finite $\tau_\hbar$ means that quantum and classical dynamics cannot be equivalent for all times but does not necessarily mean that they have to be different for all $t>\tau_\hbar$. In fact, numerical simulations for the evolution of variance of the dissipative KHO show that, in some cases, quantum and classical calculations show the same final stationary behavior but with different transient regimes as can be seen in Fig. 9. One should note, however, that this is not necessarily true for the whole phase space distributions, which can be different, although they have the same second moments. This can be illustrated through a comparison of the Wigner function depicted in Fig. 10 and the strange attractor shown in Fig. 4. The quantum distribution clearly does not exhibit all the structures presented in the classical case despite the fact that it lies in the region that contains the classical attractor.

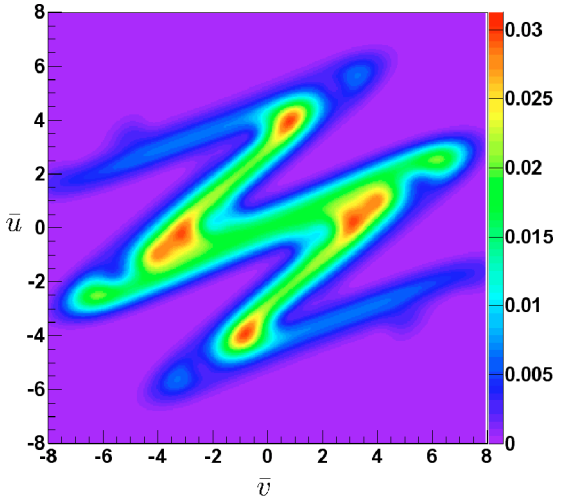

FIG. 10. (Color online) Wigner function for the same parameters of the strange attractor in Fig. 4 and $\eta=0.5$. The quantum distribution, although lying in the region of the classical attractor, does not show classical small-scale structures.

C. Diffusive environment

Evolution of the system under the influence of the diffusive environment can be solved analytically in terms of the characteristic function, described in Appendix B. The solution between consecutive kicks can be written as

$$C(\lambda,\lambda^*,t) = C(\lambda,\lambda^*,0)e^{-\gamma|\lambda|^2\tau}. \tag{42}$$

Using this solution together with Eq. (33), we can establish a recurrence relation for the characteristic function after the nth kick to be

$$C_n(\lambda,\lambda^*) = e^{-\gamma|\lambda|^2\tau}\sum_{m_1=-\infty}^{\infty} J_{m_1}(z_1)C_{n-1}(\lambda_1,\lambda_1^*), \tag{43}$$

with all the variables defined the same as in Eq. (34).

While in the dissipative case the drift effect adds an exponential factor to arguments of the Bessel functions, in this case, a Gaussian multiplies the whole sum. This difference is crucial to understanding the influence of this environment in restoring the quantum-classical correspondence. First, one should note that the role played by the Lamb–Dicke parameter in the above expressions is the same as in the case of a system without a reservoir and, therefore, the macroscopic approximation would lead to the same result as before. It is clear, however, that diffusion should have an important effect on the behavior of the system. This can be seen through a more careful analysis of expression (43).

Assume that quantum and classical dynamics coincide at kick n and forget, for the moment, diffusion. As discussed before, the two dynamics will differ as long as the approximation $\sin(\xi)\approx\xi$ fails. This gives an estimate of the values of ξ_1 that lead to quantum corrections,

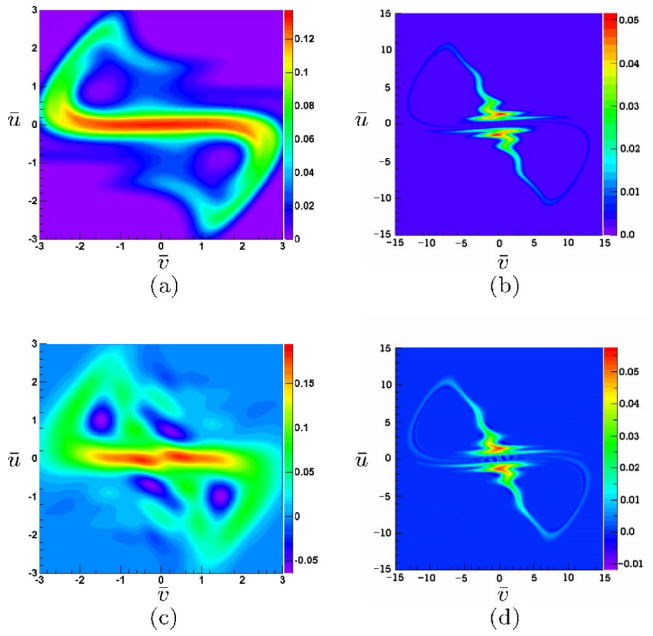

FIG. 11. (Color online) Classical (top panels) and Wigner (bottom panels) distributions for $K=2.0$, $D=0.010\,47$ and $\eta=0.5$ (left panels) or $\eta=0.1$ (right panels). Diffusion leads to better quantum-classical correspondence compared to that in Fig. 5. For $\eta=0.1$ this correspondence is quite impressive while for $\eta=0.5$ differences still remain. Diffusion also prevents the appearance of small-scale structures on classical dynamics (top).

$$|\xi_1| = \left|\frac{\eta}{2}(\lambda_1+\lambda_1^*)\right| \gtrsim 1. \tag{44}$$

This equation shows that quantum corrections are associated with large values of λ and we can define typical values λ_T for which the corrections appear as

$$|\lambda_T| \equiv |\Re(\lambda e^{i\alpha})| \gtrsim \frac{2}{\eta}. \tag{45}$$

The effect of diffusion is to cut off contributions from large values of λ, due to Gaussian modulation in Eq. (42). This implies that the values of λ that satisfy Eq. (45) may be attenuated by the Gaussian prefactor, which renders them inefficient in promoting quantum-classical separation.

This may become more intuitive if we go back from the characteristic to the Wigner function: because they are related by a Fourier transform, the larger values of the characteristic function correspond to the small-scale interference structures in the Wigner function and thus to quantum corrections. The disappearance of these small-scale structures, due to Gaussian modulation of the characteristic function, has been extensively discussed in the literature [11–15]: it leads to better correspondence between quantum and classical distributions, and to emergence of the classical world [38]. Figure 11 shows, for two different Lamb–Dicke parameters, classical and Wigner distributions in the presence of diffusion. These distributions are much more similar to each other than the corresponding distributions for the system without a reservoir displayed in Fig. 5. The importance of

diffusive effects will depend, however, on the value of the effective Planck constant, as can be seen by comparing the impressive correspondence between quantum and classical distributions for $\eta=0.1$ (right panels) and some evident differences that persist for $\eta=0.5$ (left panels).

Although it is hard to precisely define the value of diffusion needed to restore the classical limit, a rough estimate can be obtained as follows: if the values of λ_T, given by Eq. (45) lie outside the range defined by the width of the Gaussian, then the corrections should remain small. Using Eq. (45), this conditions reads

$$\frac{2}{\eta} \gtrsim \frac{1}{2\sqrt{D}}, \tag{46}$$

where $D \equiv \gamma\tau/2$ plays the role of a dimensionless diffusion coefficient for the renormalized coordinates $(\overline{u},\overline{v})$. This simple argument shows that there is a critical diffusion for which the classical and quantum dynamics remain close to each other, and that it scales as

$$D_{\mathrm{cr}} \propto \eta^2. \tag{47}$$

In terms of the diffusion coefficient in Eq. (13), one has

$$\mathcal{D}_{\mathrm{cr}} \propto \eta^4/\tau. \tag{48}$$

This is the diffusion coefficient that corresponds to nonrenormalized variables v and u. This result is consistent with those found, for example, in Refs. [11] and [14]. One should expect, however, that the strength of the nonlinearity, represented by K in our case, should play an important role in such a scaling law. The argument leading to Eq. (47) was based on estimation of the values of ξ_1 at which quantum corrections become important, without taking into account the size of these corrections. We have not studied in detail the actual separation between the two distributions as they evolve in time. That is the reason why our simple argument could not account for the influence of nonlinearity, which is hidden in Eq. (47). A detailed investigation of the separation time for the diffusive case or estimation of the error introduced by the neglected contributions would certainly display this dependence. Scaling relations between effective Planck constants, environment and nonlinearity strengths in the context of the quantum-classical transition have been obtained by many authors [7,10–13] and have motivated recent interest [14] in finding the properties of such scaling.

The above considerations suggest that the breaking time should diverge when the diffusion coefficient exceeds a certain critical value D_{cr}. This may be easily understood from Fig. 12, which displays the time evolution of the relative distance for quantum and classical variances for several values of D. One should note that, as D becomes larger than a critical value, which depends on the threshold ϵ adopted for definition of the separation time, the relative distance always remains smaller than this threshold, implying an infinite separation time. On the other hand, for sufficiently small diffusion coefficients, one should recover the logarithmic time scale. Although we were not able to derive an analytical expression for the breaking time when $D<D_{\mathrm{cr}}$, our numerical simulations show that it remains practically identical to the result obtained when no reservoir is present in this region of parameters.

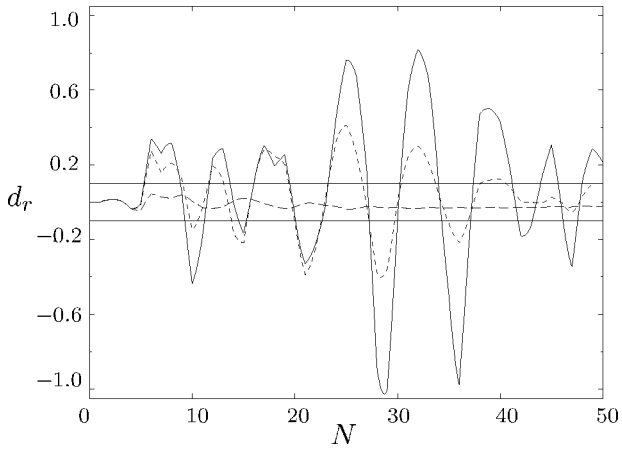

FIG. 12. Relative difference between quantum and classical variances as a function of the number of kicks for $\eta=0.5$ and D equal to 0 (solid line); 0.002 09 (dashed line) and 0.0209 (long-dashed line). For large enough D, the relative difference always remains smaller than the threshold ϵ represented by the horizontal lines.

The behavior of the breaking time in a diffusive environment is shown in Fig. 13. For $D=0.010\,47$ (top), one can see that the breaking time basically lies on the curve that corresponds to the system without a reservoir, and increases abruptly at a given value of Lamb–Dicke parameter ($\eta=0.31$, indicated by the arrow in Fig. 13), with some of the oscillations, already present in the $D=0$ case, amplified. For $\eta \leqslant 0.31$, the breaking time experiences sudden growth; corresponding points are not shown (numerical tests were performed for a maximum of 50 kicks up to $\eta=0.2$). For $\eta=0.5$ (bottom), the increase in noise introduces very small changes in the breaking time, which grows quickly when $D \approx 0.014\,66$. Again the abrupt increase indicates that the differences between quantum and classical variances remain bounded below a given limit ϵ.

One should note, however, that the small changes in the breaking time for $D<D_{\mathrm{cr}}$ do not imply that the environment has no effect at all in the dynamics. In fact, by observing Fig. 12 again we see that the maximum distance between the variances decreases smoothly with an increase in noise strength and may eventually be zero, indicating perfect quantum-classical correspondence. It is interesting to note how these two different quantities, breaking time and maximum distance, give complementary information about the dynamics.

From these results one could infer, naively, that diffusion is sufficient to restore the classical limit for a chaotic system no matter what the value of the effective Planck constant is. Indeed, for a given Lamb–Dicke parameter, one can always find a large enough diffusion coefficient to bring the quantum and classical dynamics sufficiently close to each other. Nevertheless, such a statement deserves some reservation. In fact, diffusion washes out not only the interference pattern in the Wigner function but also the structures in classical phase

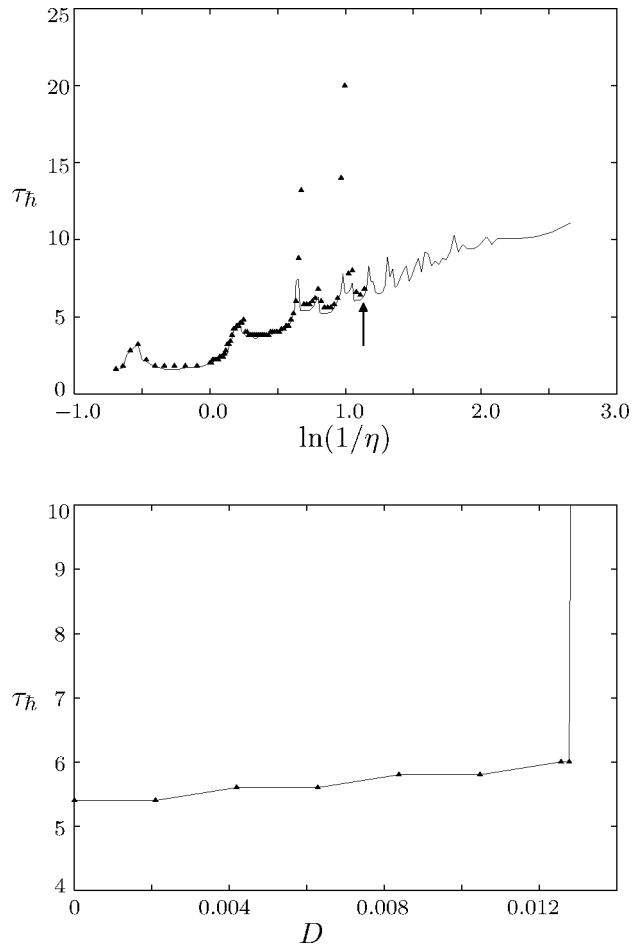

FIG. 13. Top: Breaking time as function of $\ln(1/\eta)$ for $D=0.010\,47$ (triangles) and $D=0$ (line). The two curves are essentially the same until $\eta \approx 0.31$ (shown by the arrow) when there is no longer any separation. Some peaks of the $D=0$ curve are amplified, due, probably, to the definition of breaking time adopted. Bottom: Breaking time as function of D for $\eta=0.5$. The separation time remains basically the same, with a small increase ($\approx$10% maximum), and suddenly increases for $D_{cr} \approx 0.13$.

space (see Fig. 11), and one could claim, therefore, that when the critical diffusion coefficient is very large, the chaotic characteristic of the system is lost and the system follows, basically, diffusive dynamics induced by the environment. A similar situation was described in the dissipative case where large enough dissipation was sufficient to suppress chaos and bring the system to periodic behavior. There, however, we could clearly distinguish between chaotic and periodic behavior through calculation of the Lyapunov exponent, while here, even though generalizations of Lyapunov exponents for distributions exist [39,40], there is no sharp distinction between chaotic and regular behavior. Description of the system can become even more complicated with the addition of diffusion in view of the mixed phase-space structure of the system. Difficulties in characterizing chaos lie not only in smoothing the phase space structures [see Fig. 11(a)], but also in the fact that the distribution can flow from regular to chaotic regions that were well separated when no reservoirs are taken into account.

Finally, we should remark that we have not analyzed here long-time behavior of the system. It is well known that diffusion may affect quantum localization, which occurs at times much longer than those considered here [7–10]. In the absence of a reservoir, the long-time dynamics of the model analyzed in this paper may display either quantum diffusion or ballistic behavior [16].

V. CONCLUSIONS

We have shown that it is possible to discuss separately, in a physically relevant way, the roles of the macroscopic limit and of different system–environment interactions in the quantum-classical transition of a chaotic system. We have considered the kicked harmonic oscillator coupled to two distinct reservoirs that give rise in the classical limit to either pure dissipation (zero-temperature reservoir) or pure diffusion (random force) in a situation that could be implemented in state-of-the-art ion trap experiments.

In the chaotic regime, when interaction with a reservoir is not taken into account, the classical and quantum dynamics start diverging after a time that depends logarithmically on the ratio between a typical action of the system and the Planck constant. We have used an operational definition of the breaking time in terms of measurable quantities, which allows experimental testing of this logarithmic time scale.

In the dissipative case we established regions of parameters that correspond to different time scales. There is a region where quantum corrections appear right after the first kick and quantum-classical correspondence is already lost at the beginning of evolution. By decreasing the Lamb–Dicke parameter, one reaches a region where quantum-classical correspondence persists for a time that, like in the system without a reservoir, grows only logarithmically with the classicality parameter. We have also shown that, for a fixed effective Planck constant, close agreement between quantum and classical predictions is only possible for dissipation strengths large enough to bring the system into regular behavior.

In the diffusive case, we were able to establish that the behavior of the quantum-classical separation should be markedly different, depending on whether the diffusion coefficient is above or below a certain critical value D_{cr}. For $D > D_{cr}$, this separation should remain small, and infinite separation times may even be obtained, at values of D that depend on the definition adopted for critical percentual separation. We have also presented numerical evidence that, for diffusion coefficients below this limit, the breaking time behaves like that in the case without a reservoir. Furthermore, we obtained an analytical estimate of the dependence of the critical diffusion coefficient on the effective Planck constant, which shows that the farther away from the classical limit the system is, the larger the effect of the environment must be to restore quantum-classical correspondence.

Although coupling with the environment helps to restore quantum-classical correspondence for a system that is close to the macroscopic regime, for systems in a deep quantum region critical diffusion can be so large that it brings classicality at the expense of reducing, or even extinguishing, chaotic features of the system.

The behavior of the system under the influence of other kinds of environment could also be explored in this context. Thermal and phase reservoirs are examples of different environments, already produced in ion trap experiments, that could be used for this, and could lead to interesting results for the quantum-classical transition scenario.

ACKNOWLEDGMENTS

One of the authors (A.R.R.C.) thanks A. Buchleitner and S. Wimberger for many useful discussions and H. Häffner for comments on experimental issues. This work was partially supported by the Programa de Apoio a Núcleos de Excelência (PRONEX), the Conselho Nacional de Desenvolvimento Científico e Tecnológico (CNPq), Fundação de Amparo à Pesquisa do Estado do Rio de Janeiro (FAPERJ), Fundação Universitária José Bonifácio (FUJB), and the Brazilian Millennium Institute for Quantum Information.

APPENDIX A: BREAKING TIME

It is not difficult to generalize the solutions, Eqs. (33) and (34), which were obtained for the characteristic function corresponding to a system without a reservoir, to the dissipative regime. Between two consecutive kicks the harmonic evolution just rotates the system in phase space, and this effect appears only in the complex exponential in Eq. (34a). Solution of the dissipative master equation simply adds exponential decay $e^{-\Gamma\tau/2}$ [37] and, therefore, solution of the full problem is still given by Eq. (33):

$$C_n(\lambda,\lambda^*) = \sum_{m_1,\ldots,m_n=-\infty}^{\infty} J_{m_1}(z_1)J_{m_2}(z_2)\ldots J_{m_n}(z_n)C_0(\lambda_n,\lambda_n^*), \tag{A1}$$

where

$$\lambda_k = \lambda_{k-1}e^{i\bar{\alpha}}e^{-\Gamma\tau/2} + i2m_k\eta, \tag{A2a}$$

$$z_k = 2K_q\sin(\xi_k) = \frac{K'}{\eta^2}\sin(\xi_k), \tag{A2b}$$

$$\xi_k = -\frac{\eta}{2}(\lambda_k + \lambda_k^*), \tag{A2c}$$

$$\lambda_0 \equiv \lambda. \tag{A2d}$$

The procedure to obtain the breaking time in the dissipative case follows very closely the one used in Ref. [18] for the situation without a reservoir. First we should note that the macroscopic limit, as discussed previously, is achieved by letting $\eta\to 0$, which means that the sine functions in Eq. (A2b) can be approximated by their argument, i.e.,

$$\sin(\xi_k) \approx \xi_k. \tag{A3}$$

In this limit, we obtain the semiclassical characteristic function,

$$C_n(\lambda,\lambda^*) = \sum_{m_1,\ldots,m_n=-\infty}^{\infty} J_{m_1}(2K_q\xi_1)\ldots J_{m_n}(2K_q\xi_n)C_0(\lambda_n,\lambda_n^*), \tag{A4}$$

with initial condition

$$C_0^{cl}(\lambda,\lambda^*) = \int_{-\infty}^{\infty} d^2\mu P_0(\mu,\mu^*)e^{\lambda_n\mu^* - \lambda_n^*\mu}. \tag{A5}$$

When no reservoir is present, the semiclassical approximation leads to the classical characteristic function derived, directly, through the corresponding classical map. Here this is not the case, due to the fact that the zero-temperature reservoir leads to distinct features in the quantum and the classical models. If subjected only to the dissipative dynamics, the quantum system will end up in its ground state, which has a finite width, while a classical probability distribution would contract to a point located at the origin. In this way, the semiclassical characteristic function shows exactly the same nonlinear dynamics as the classical but with an intrinsic quantum property due to the uncertainty principle. Of course, this effect becomes smaller as quantum fluctuations become negligible compared to the size of the system, which occurs for small values of Lamb–Dicke parameter.

The replacement of Eq. (33) by Eq. (A4) is only valid if Eq. (A3) holds for every k. Taking into account that the Bessel functions decrease exponentially for $|m_k| \gg 2K_q\xi_k$, we can truncate the sums in Eq. (A1) by estimating the maximum values of $|m_k|$ in each sum. The relevant contributions are the ones in which the Bessel function index is of the order of its argument and, therefore,

$$|m_1| \approx 2K_q|\xi_1| = \frac{K'}{2\eta}e^{-\Gamma\tau/2}|\lambda e^{i\bar{\alpha}} + \lambda^* e^{-i\bar{\alpha}}|,$$

$$|m_2| \approx 2K_q|\xi_2| = \frac{K'}{2\eta}|(\lambda e^{i2\bar{\alpha}} + \lambda^* e^{-i2\bar{\alpha}})e^{-2\Gamma\tau/2} - 2m_1\eta\sin(\bar{\alpha})e^{-\Gamma\tau/2}|,$$

$$|m_n| \approx 2K_q|\xi_n| = \frac{K'}{2\eta}|(\lambda e^{in\bar{\alpha}} + \lambda^* e^{-in\bar{\alpha}})e^{-n\Gamma\tau/2} - 2m_1\eta\sin[(n-1)\bar{\alpha}]e^{-(n-1)\Gamma\tau/2} - \ldots - 2m_{n-1}\eta\sin(\bar{\alpha})e^{-\Gamma\tau/2}|.$$

Considering now the strong chaos limit ($K' \gg 1$), we have

$$|m_1| \approx \frac{\bar{K'}}{2\eta\sin(\bar{\alpha})}e^{-\Gamma\tau/2}, \ldots, \quad |m_n| \approx \frac{\bar{K'}^n}{2\eta\sin(\bar{\alpha})}e^{-n\Gamma\tau/2}.$$

From the above considerations we can study the regime of validity of the approximation $|\xi_k| \ll 1$ for all k. The ratio between two consecutive ξ is given by

$$\frac{|\xi_k|}{|\xi_{k-1}|} \approx \bar{K'}e^{-\Gamma\tau/2}, \tag{A6}$$

while the first argument is

$$|\xi_1| \approx \frac{\eta e^{-\Gamma\tau/2}}{2}. \tag{A7}$$

From Eq. (A7) we can get two different conditions on the first argument $|\xi_1|$. If $\Gamma\tau/2 < \ln(\eta/2)$ then $|\xi_1| > 1$ and, right after the first kick, the classical approximation is not valid any longer, so quantum predictions should differ from classical ones. This corresponds to the results shown in the first column of Table I which are represented by $\tau_\hbar^{\rm dis} \approx 1$ kick. If, on the other hand, $\Gamma\tau/2 > \ln(\eta/2)$ and, therefore, $|\xi_1| < 1$, then we have two new possibilities depending on condition (A6).

By choosing $\Gamma\tau/2 > \ln(\overline{K'})$, the ratio between two consecutive ξ is less than one and the sequence of ξ_k's decreases with an increase of k. Because $|\xi_1| < 1$, all the terms will be smaller than one and quantum and classical evolutions should stay close to each other at all times ($\tau_\hbar^{\rm dis} \to \infty$). Nevertheless, if we have $\Gamma\tau/2 < \ln(\overline{K'})$ the sequence of ξ_k's increases and one should expect that there is a ξ_k for which the condition $|\xi_k| < 1$ is not fulfilled any longer and a breaking time will exist. This will happen when $|\xi_k| \approx 1$, which can be expressed as

$$\frac{\overline{K'}^n \eta e^{-n\Gamma\tau/2}}{2\overline{K'}} \approx 1. \tag{A8}$$

Taking the logarithm and noting that n, the number of kicks, corresponds to the time in units of τ, we arrive at an estimate for the breaking time as

$$\tau_\hbar^{\rm dis} \equiv n \approx \frac{\ln(2\overline{K'}/\eta)}{\ln(\overline{K'}) - \Gamma\tau/2}. \tag{A9}$$

APPENDIX B: DIFFUSIVE CASE

The evolution of the symmetrically ordered characteristic function defined in Eq. (32) is given by

$$\dot{C}(\lambda,\lambda^*) = \mathrm{Tr}[\dot{\hat{\rho}} e^{\lambda\hat{a}^\dagger - \lambda^*\hat{a}}]. \tag{B1}$$

The diffusive dynamics is now introduced by the replacement of $\dot{\hat{\rho}}$ in the above equation by Eq. (29), which gives

$$\dot{C}(\lambda,\lambda^*) = \frac{\gamma}{2}\mathrm{Tr}[-\hat{a}^\dagger\hat{a}\rho e^{\lambda\hat{a}^\dagger - \lambda^*\hat{a}} + 2\hat{a}\rho\hat{a}^\dagger e^{\lambda\hat{a}^\dagger - \lambda^*\hat{a}} - \rho\hat{a}^\dagger\hat{a}e^{\lambda\hat{a}^\dagger - \lambda^*\hat{a}} - \hat{a}\hat{a}^\dagger\rho e^{\lambda\hat{a}^\dagger - \lambda^*\hat{a}} + 2\hat{a}^\dagger\rho\hat{a}e^{\lambda\hat{a}^\dagger - \lambda^*\hat{a}} - \rho\hat{a}\hat{a}^\dagger e^{\lambda\hat{a}^\dagger - \lambda^*\hat{a}}]. \tag{B2}$$

Rewriting the exponentials using the Baker–Hausdorff formula and ordering properties,

$$e^{-\beta\hat{a}^\dagger} f(\hat{a},\hat{a}^\dagger) e^{\beta\hat{a}^\dagger} = f(\hat{a}+\beta,\hat{a}^\dagger), \tag{B3a}$$

$$e^{\beta\hat{a}} f(\hat{a},\hat{a}^\dagger) e^{-\beta\hat{a}} = f(\hat{a},\hat{a}^\dagger+\beta), \tag{B3b}$$

we obtain

$$\dot{C}(\lambda,\lambda^*) = \frac{\gamma}{2}\mathrm{Tr}[-2|\lambda|^2 e^{\lambda\hat{a}^\dagger - \lambda^*\hat{a}}\hat{\rho}] = -\Gamma|\lambda|^2 C(\lambda,\lambda^*). \tag{B4}$$

This equation can be readily integrated, giving as a solution,

$$C(\lambda,\lambda^*,t) = C(\lambda,\lambda^*,0)e^{-\gamma|\lambda|^2 t}. \tag{B5}$$

[1] G. P. Berman and G. M. Zaslavsky, Physica A **91**, 450 (1978).
[2] W. H. Zurek, Acta Phys. Pol. B **29**, 3689 (1998).
[3] M. Berry, in *Quantum Mechanics: Scientific Perpectives on Divine Action*, edited by K. W.-M. Robert John Russell, Philip Clayton, and J. Polkinghorne (Vatican Observatory, Center for Theology and Natural Sciences, 2001), pp. 41–54.
[4] R. P. Feynman and F. L. Vernon, Ann. Phys. (N.Y.) **24**, 118 (1963).
[5] A. O. Caldeira and A. J. Leggett, Physica A **121**, 587 (1983).
[6] A. O. Caldeira and A. J. Leggett, Ann. Phys. (N.Y.) **149**, 374 (1983).
[7] E. Ott, T. M. Antonsen, and J. D. Hanson, Phys. Rev. Lett. **53**, 2187 (1984).
[8] T. Dittrich and R. Graham, Ann. Phys. (N.Y.) **200**, 363 (1990).
[9] M. Wilkinson and E. J. Austin, Phys. Rev. A **46**, 64 (1992).
[10] D. Cohen, J. Phys. A **27**, 4805 (1994).
[11] A. R. Kolovsky, Phys. Rev. Lett. **76**, 340 (1996).
[12] W. H. Zurek and J. P. Paz, Phys. Rev. Lett. **72**, 2508 (1994).
[13] A. K. Pattanayak, Phys. Rev. Lett. **83**, 4526 (1999).
[14] A. K. Pattanayak, B. Sundaram, and B. D. Greenbaum, Phys. Rev. Lett. **90**, 014103 (2003).
[15] S. Habib, K. Shizume, and W. H. Zurek, Phys. Rev. Lett. **80**, 4361 (1998).
[16] F. Borgonovi and L. Rebuzzini, Phys. Rev. E **52**, 2302 (1995).
[17] G. M. Zaslavsky, R. Z. Sagdeev, D. A. Usikov, and A. A. Chernikov, *Weak Chaos and Quasi-regular Patterns* (Cambridge University Press, Cambridge, 1992).
[18] G. P. Berman, V. Y. Rubaev, and G. M. Zaslavsky, Nonlinearity **4**, 543 (1991).
[19] B. Hu, B. Li, J. Liu, and J. L. Zhou, Phys. Rev. E **58**, 1743 (1998).
[20] S. A. Gardiner, J. I. Cirac, and P. Zoller, Phys. Rev. Lett. **79**, 4790 (1997).
[21] J. F. Poyatos, J. I. Cirac, and P. Zoller, Phys. Rev. Lett. **77**, 4728 (1996).
[22] Q. A. Turchette, C. J. Myatt, B. E. King, C. A. Sackett, D. Kielpinski, W. M. Itano, C. Monroe, and D. J. Wineland, Phys. Rev. A **62**, 053807 (2000).
[23] A. Iomin and G. M. Zaslavsky, Phys. Rev. E **67**, 027203 (2003).
[24] A. A. Chernikov, R. Z. Sagdeev, and G. M. Zaslavsky, Physica D **33**, 65 (1988).
[25] A. A. Vasiliev, G. M. Zaslavsky, M. Y. Natenzon, A. I. Neishtadt, B. A. Petrovichev, R. Z. Sagdeev, and A. A. Chernikov,

Sov. Phys. JETP **67**, 2053 (1989).
[26] A. Lasota and M. C. Mackey, *Chaos, Fractals and Noise* (Springer-Verlag, New York, 1994).
[27] R. F. Fox, Chaos **5**, 619 (1995).
[28] A. J. Lichtenberg and M. A. Lieberman, *Regular and Chaotic Dynamics* (Springer-Verlag, New York, 1994).
[29] H. L. S. Alan Wolf, J. B. Swift, and J. A. Vastano, Physica D **16**, 285 (1985).
[30] D. J. Wineland, C. Monroe, W. M. Itano, D. Leibfried, B. E. King, and D. M. Meekhof, J. Res. Natl. Inst. Stand. Technol. **103**, 29 (1998).
[31] G. Lindblad, Commun. Math. Phys. **48**, 119 (1976).
[32] R. Alicki and K. Lendi, *Quantum Dynamical Semigroups and Applications, Lecture Notes in Physics*, Vol. 286 (Springer-Verlag, Berlin, 1987).
[33] A. R. R. Carvalho, P. Milman, R. L. de Matos Filho, and L. Davidovich, Phys. Rev. Lett. **86**, 4988 (2001).
[34] D. F. V. James, Phys. Rev. Lett. **81**, 317 (1998).
[35] C. Beck and F. Schlögl, *Thermodynamics of Chaotic Systems: An Introduction* (Cambridge University Press, London, 1993).
[36] D. Leibfried, D. M. Meekhof, B. E. King, C. Monroe, W. M. Itano, and D. J. Wineland, Phys. Rev. Lett. **77**, 4281 (1996).
[37] S. M. Barnett and P. M. Radmore, *Methods in Theoretical Quantum Optics* (Oxford University Press, Oxford, 1997).
[38] W. H. Zurek, Rev. Mod. Phys. **75**, 715 (2003).
[39] Y. Gu, Phys. Lett. A **149**, 95 (1990).
[40] A. K. Pattanayak and P. Brumer, Phys. Rev. E **56**, 5174 (1997).